Materials Science and Engineering C 56 (2015) 195–204

Contents lists available at ScienceDirect

Materials Science and Engineering C

journal homepage: www.elsevier.com/locate/msec

Physio-chemical and antibacterial characteristics of pressure spun nylon nanofibres embedded with functional silver nanoparticles

Z. Xu [a], S. Mahalingam [a], J.L. Rohn [b], G. Ren [c], M. Edirisinghe [a,*]

[a] Department of Mechanical Engineering, University College London, London WC1E 7JE, UK
[b] Centre for Clinical Science and Technology, Division of Medicine, University College London, London, UK
[c] School of Engineering and Technology, University of Hertfordshire, Hatfield AL10 9AB, UK

ARTICLE INFO

Article history:
Received 19 March 2015
Received in revised form 3 June 2015
Accepted 5 June 2015
Available online 9 June 2015

Keywords:
Polymer
Nanofibres
Nanoparticles
Pressure
Gyration
Bacteria

ABSTRACT

A novel and facile approach to prepare hybrid nanoparticle embedded polymer nanofibers using pressurised gyration is presented. Silver nanoparticles and nylon polymer were used in this work. The polymer solution's physical properties, rotating speed and the working pressure had a significant influence on the fibre diameter and the morphology. Fibres in the range of 60–500 nm were spun using 10 wt.%, 15 wt.% and 20 wt.% nylon solutions and these bead-free fibres were processed under 0.2 MPa and 0.3 MPa working pressure and a rotational speed of 36,000 rpm. 1–4 wt.% of Ag was added to these nylon solutions and in the case of wt.% fibres in the range 50–150 nm were prepared using the same conditions of pressurised gyration. Successful incorporation of the Ag nanoparticles in nylon nanofibres was confirmed by using a combination of advanced microscopical techniques and Raman spectrometry was used to study the bonding characteristics of nylon and the Ag nanoparticles. Inductively coupled plasma mass spectroscopy showed a substantial concentration of Ag ions in the nylon fibre matrix which is essential for producing effective antibacterial properties. Antibacterial activity of the Ag-loaded nanofibres shows higher efficacy than nylon nanofibres for Gram-negative *Escherichia coli* and *Pseudomonas aeruginosa* microorganisms, and both Ag nanoparticles and the Ag ions were found to be the reason for enhanced cell death in the bacterial solutions.

1. Introduction

Hybrid nanofibres are an interesting class of materials currently receiving significant attention due to their unique chemical, electrical, optical and mechanical properties that could be achieved by combining the advantages of nanoparticles and polymer nanofibres [1,2]. These properties enable such materials to be used in a wide range of applications including biomedical, energy storage, catalysis and sensors. Properties of the hybrid nanofibres not only depend on the high surface area to volume ratio of the polymer nanofibres but also the content, size and spatial distribution of the nanoparticles [3,4].

The development of hybrid nanofibres is of tremendous interest for the biomedical research community because scaffolds prepared from such materials resemble natural extracellular matrices with very good mechanical strength, biocompatibility and biodegradability with respect to various human cells and tissues [5,6]. Nanofibrous structures as an antimicrobial scaffold provide higher cell adhesion than other structures [7]. They have been also used in wound dressing and healing where these scaffolds possess more homogeneity, oxygen penetration and prevent infections and dehydration [8]. Nylon polymer nanofibres exhibit excellent mechanical properties, such as toughness, and high tensile strength and have been adopted to make various composites [9–11]. Ag nanoparticles show excellent antibacterial activity and have a tolerant range of cytotoxicity, strong inhibitory and bactericidal effects [12–14]. Ag belongs to an interesting group of antimicrobials that exhibit greater thermal stability and long term activity [15]. In addition, Ag has commanded much attention among all the antimicrobials because it not only provides intensive antimicrobial properties but also possesses acceptable cytotoxicity towards mammalian cells and tissues [16]. It has been reported that Ag nanoparticle embedded nanofibres showed enhanced antimicrobial efficacy against Gram-positive and Gram-negative bacteria [17,18]. Thus, ZnO and Ag nanoparticles were used for filling polymers such as polyurethane for making nanofibres which have demonstrated a high degree of antibacterial-activities [19].

Pressurised gyration is a simple and versatile mass production technique of nanofibres and nanofibrous structures with controllable fibre size and fibre size distribution. The technique consists of a vessel containing polymer solution subjected to simultaneous centrifugal force and dynamic fluid flow in order to extrude fibres with tailored morphologies and functionality [20]. The nanofibres produced through this technique depend on the rotating speed of the vessel, air pressure and the concentration of polymer solution. Unlike electrospinning it is a nozzle free method independent of the electrical conductivity and the

* Corresponding author.
E-mail address: m.edirisinghe@ucl.ac.uk (M. Edirisinghe).

http://dx.doi.org/10.1016/j.msec.2015.06.003

dielectric constant of polymer solution. The process offers production of fine long continuous fibres in a well oriented direction. The highly oriented nanofibres produced can provide mechanically stronger fibres with remarkable surface active areas [21,22].

The influence of the processing parameters such as vessel rotating speed, air pressure and the nylon concentration in the solutions on the fibre size and the size distribution were investigated in this work. Surface morphology studies and chemical analysis were carried out on the nanofibres. The antibacterial activities of nylon and Ag-loaded nylon nanofibres were studied by using *Escherichia coli* and *Pseudomonas aeruginosa* tested in aerobic suspension cultures. These hybrid nanofibres could be utilised for a wide range of biological applications, such as antibacterial wound dressing, functional scaffolds for tissue engineering, and antibacterial water and air filtration devices and systems.

2. Experimental details

2.1. Materials

Nylon 6,6 (pellets, molecular weight ~ 30,000 g/mol, density 1.18 g/ml, laboratory grade), formic acid (analytical grade) and aqueous silver nanoparticles (particle size < 150 nm) were purchased from Sigma-Aldrich (Poole, UK). All reagents were used without further purification.

2.2. Preparation of nylon and Ag-loaded nylon solutions

Nylon solutions modified with functional Ag nanoparticles were prepared and used in conjunction with nylon only solutions for comparison. The polymer solutions were prepared in an air-tight bottle using formic acid as solvent to dissolve the nylon pellets under magnetic stirring for ~24 h at ambient temperature (~20 °C). Four different concentrations of nylon (5, 10, 15, and 20% w/w) were prepared. Ag containing nylon solutions were prepared by adding 1 wt.% of aqueous silver nanoparticle suspension to the nylon solutions. These were also prepared using a magnetic stirrer in an air-tight bottle at the ambient temperature. Similarly, 2 wt.% and 4 wt.% Ag nanoparticle containing nylon solutions were prepared for making nanofibres and these were only tested for Ag-ion release in aqueous solution (see Section 2.4).

2.3. Pressurised gyration

Details of the experimental set-up of the pressurised gyration process accompanied by videos and illustrating the process in depth; including jet initiation, instability and mass production of nanofibres, are reported in our previous work [20].

2.4. Characterisation

Solution physical properties such as surface tension and viscosity are crucial in pressurised gyration fibre forming [20]. The surface tension and the viscosity of all the solutions were measured using a KRUSS tensiometer and a Brookfield viscometer, respectively, at ambient temperature as listed in Table 1.

Table 1
Measured values of surface tension and viscosity for nylon solutions.

Nylon system solutions	Surface tension (mN/m)	Viscosity (mPa s)
5 wt.% nylon	38.3(±2.4)	53.5(±0.3)
10 wt.% nylon	42.7(±2.7)	236.9(±0.7)
15 wt.% nylon	52.1(±2.5)	461.1(±2.7)
20 wt.% nylon	73.5(±3.4)	2016.4(±14.6)
5 wt.% nylon + 1% Ag	38.2(±0.9)	29.8(±0.2)
10 wt.% nylon + 1% Ag	41.3(±1.2)	181.1(±2.1)
15 wt.% nylon + 1% Ag	49.7(±3.2)	245.6(±2.7)
20 wt.% nylon + 1% Ag	66.4(±5.2)	924.9(±5.0)

The characteristics and the morphology of nanofibres were studied using field emission scanning electron microscopy (FE-SEM) – energy dispersive x-ray spectroscopy (EDX) and focussed ion beam microscopy (Carl Zeiss-Gemini). Nanofibre samples were coated with gold using a sputtering machine (sputter time ~75 s) before loading in to the microscopes. High and low magnification images were acquired in randomly selected positions (>20) within a sample. The fibre diameter was obtained using Image J software. About 150 measurements were made at random locations to plot the fibre diameter distribution.

Raman spectra of nylon (20 wt.%) and Ag-loaded nylon samples (Ag concentration was 1 wt.% and 4 wt.%) were obtained using a Renishaw Raman microscope excited with 514.5 nm incident wavelength radiation. The data acquisition covered the spectral range 2000–100 cm^{-1} with a spatial resolution of 4 cm^{-1}.

The Ag ion release from Ag-loaded nanofibrous mats obtained from 20 wt.% nylon was tested with inductively coupled plasma mass spectroscopy (ICP-MS, Agilent, Japan). The Ag concentration was 1 wt.%, 2 wt.% and 4 wt.% in the nanofibres. The prepared samples were cut into appropriate size and were washed in de-ionised water (30 ml) for 24, 48 and 72 h in each case. Then they were immersed in 1 wt.% nitric acid (HNO_3), which was used as a stock solution. For comparative and calibration purposes the de-ionised water and nitric acid were screened using ICP-MS for Ag ion content. Thus, the Ag ion concentration in the releasing medium was quantified and for each case three measurements were made.

2.5. Antibacterial testing

In order to investigate the antibacterial activities of the nylon (20 wt.%) and Ag-loaded nanofibres, antibacterial performance tests were conducted. For this purpose, two Gram-negative bacteria, *E. coli* (in house strain number 3891) and *P. aeruginosa* (strain 25-09071215-05) were used. Bacterial broth suspensions were co-cultured under aerobic conditions with the sample for set periods of time, after which the number of viable colony-forming units (CFU) of bacteria was obtained and then the antibacterial rate for each sample was calculated.

Due to strong bactericidal activity of formic acid, all of the nanofibre samples for the antibacterial tests were washed with distilled water (pH 6.5) for 96 h to remove any residual formic acid. Post-washing, the pH value of nylon nanofibres was ~6 and those of the Ag-loaded nylon nanofibres was ~5. The assay was performed using bacteria cultured overnight from a single colony to stationary phase (approximately 10^9 CFU/ml) in Luria-Bertani (LB) broth in a shaking aerobic incubator at 37 °C. Next, a suspension, ~5×10^5 CFU/ml in LB, was prepared for use as the experimental bacterial suspension working in a sterile laminar flow hood environment.

The same weight of nanofibre samples (0.02 g) in a constant liquid volume (0.02 ml) was placed using sterile tweezers into each well of a 24-well tissue culture plate (Corning) along with 0.5 ml of the experimental bacterial suspension of either *E. coli* or *P. aeruginosa.* In these tests, 10 samples were tested for each bacterium, 5 samples of nylon nanofibres and 5 samples of Ag-loaded nylon nanofibres. Wells with experimental suspension alone containing no sample were also used as a negative control. The plates were cultured in an aerobic shaking incubator at 37 °C for 2 h and 24 h. After co-culturing with the samples, the bacterial suspensions were diluted (1:1, 1:10, 1:100 and 1:1000) into sterile tubes, after which 0.02 ml each dilution was applied evenly onto quadrants of chromogenic agar plates (chromID CPS, Biomerieux) for enumeration using sterile L-spreaders. Chromogenic agar allows confirmation of bacterial species by colony colour. The plates were incubated overnight at 37 °C for 24 h. Finally, the number of bacteria colonies (CFU) on each quadrant was counted to evaluate the effect of the original sample on survival of the bacteria.

The antibacterial rate of a material can be determined by AR (%) = $[(N_1 - N_2) / N_1] \times 100$, where, AR is the antibacterial ratio (%); N_1 is

the bacterial count of the negative control and N_2 is the bacterial count of the antibacterial nanofibres [23]. The morphological characteristics of the bacterial cells cultured onto the nanofibres were also investigated. For this purpose, bacterial cells were co-cultured with nanofibres as in the above assay and incubated at 37 °C for 24 h. Following incubation, nanofibres were washed three times with phosphate-buffered saline (PBS) to remove unbound and loosely adhered bacteria. Subsequently, they were stained with 33% methylene blue in PBS solution for 10 min and observed using a light microscope (Olympus).

3. Results and discussion

In pressurised gyration, rotating speed and working pressure of the solution being spun can determine the morphology of the product [24] and therefore careful selection of the operation region has to be selected. The physical properties of the polymer solutions significantly influence the jet formation and fibre formation during pressurised gyration. The surface tension and viscosity of nylon solutions increased with nylon concentration (Table 1). For 20 wt.% nylon, the surface tension was ~74 mN/m which is nearly double the value of 5 wt.% nylon solution. The viscosity of 20 wt.% nylon solution was ~2016 mPa s which was more than an order of magnitude higher than that of the value at 10 wt.% nylon. Similarly, the surface tension and viscosity were increased with the solute content in the Ag-loaded nylon suspensions. It should be noted that, the viscosities of Ag-loaded nylon suspensions decreased compared to the nylon only counterparts because, as received, Ag nanoparticles were dispersed in an organic solvent (triethylene glycol monomethyl ether) and this constituent acts like a surfactant in the Ag-nylon suspension. For a given molecular weight, the increase of viscosity with the solute content was due to an increase of chain entanglement in the polymer solution where the polymer chains overlap each other to form a strong network. At the low concentration, low viscosity was observed due to insufficient chain entanglement as a result of lack of physical interlocking of chains [25].

Fig. 1(a) and (b) shows the plots of fibre diameter against the rotating speed for 10, 15 and 20 wt.% of nylon solutions with and without 1 wt.% Ag nanoparticles-dispersed in the solutions under a fixed working pressure of 0.1 MPa. It is clearly demonstrated that the fibre diameter is significantly reduced with an increase in rotating speed of the vessel. For 20 wt.% nylon solution the fibre diameter was reduced from 470 nm to 303 nm when the rotating speed changed from 24,000 rpm to 36,000 rpm. Similarly, a 40% reduction of fibre diameter was observed for 15 wt.% of nylon solution, where the fibre diameter was reduced from 385 nm to 231 nm when the rotating speed increased from 24,000 rpm to 36,000 rpm. However, the fibre diameter was not significantly affected by the increase of rotating speed for the 10 wt.% nylon solution. For 20 wt.% and 15 wt.% Ag-loaded nylon solutions, the variation of rotating speed had a marked influence on fibre diameter (Fig. 1b). Here the fibre diameter was reduced from 152 nm to 140 nm and 128 nm to 103 nm when the rotating speed increased from 24,000 rpm to 36,000 rpm for 20 wt.% and 15 wt.%, respectively. Again, for the 10 wt.% Ag-loaded nylon solution the fibre diameter produced was not significantly changed with rotating speed and the obtained value was ~90 nm. This is likely to be due to low viscosity of

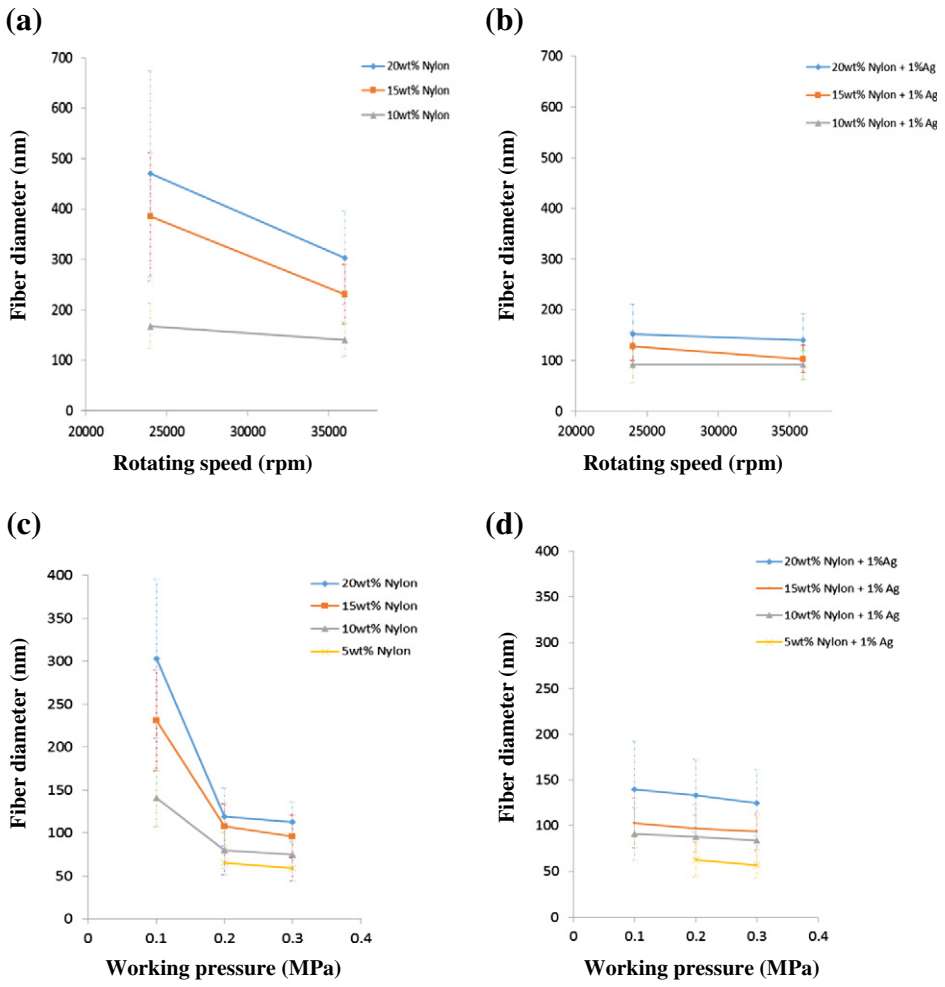

Fig. 1. Fibre diameter variation for 5 wt.%, 10 wt.%, 15 wt.% and 20 wt.% of nylon and nylon with Ag nanoparticle incorporation (a), (b) varying rotating speed at a constant working pressure of 0.1 MPa. (c), (d) Varying working pressure at a fixed rotating speed of 36,000 rpm.

Table 2
Fibre diameter variation for different conditions of pressurised gyration.

Nylon + Ag nanoparticles loading	Average fibre diameter (nm) at rotating speed (rpm); working pressure (MPa) combinations			
	24,000; 0.1	36,000; 0.1	36,000; 0.2	36,000; 0.3
5 wt.% + 0 wt.%	–	–	65	59
10 wt.% + 0 wt.%	168	141	80	75
15 wt.% + 0 wt.%	385	231	108	96
20 wt.% + 0 wt.%	470	303	119	113
5 wt.% + 1 wt.%	–	–	63	57
10 wt.% + 1 wt.%	92	91	88	84
15 wt.% + 1 wt.%	128	103	97	94
20 wt.% + 1 wt.%	152	140	133	125

polymer/Ag-solution and rapid evaporation of solvent during the spinning process. Moreover, only polymer beads were generated with the 5 wt.% nylon solution and Ag-loaded nylon solution at 0.1 MPa working pressure and low rotating speeds.

Fig. 1(c) and (d) shows graphs of fibre diameter variation with working pressure for pressurised gyration at a fixed rotating speed of 36,000 rpm for nylon and Ag-loaded nylon polymer solutions, respectively. A fibre diameter in the range of 59 nm to 303 nm was achieved for the nylon samples, and this was 57 nm to 140 nm for Ag-loaded nylon. It is clear that the increase of the working pressure dramatically reduced the fibre diameter. For 20 wt.% nylon solution the fibre diameter was reduced from 303 nm to 113 nm on increasing the working pressure from 0.1 MPa to 0.3 MPa at a rotating speed of 36,000 rpm. Similarly, the fibre diameter was reduced from 231 nm to 96 nm and

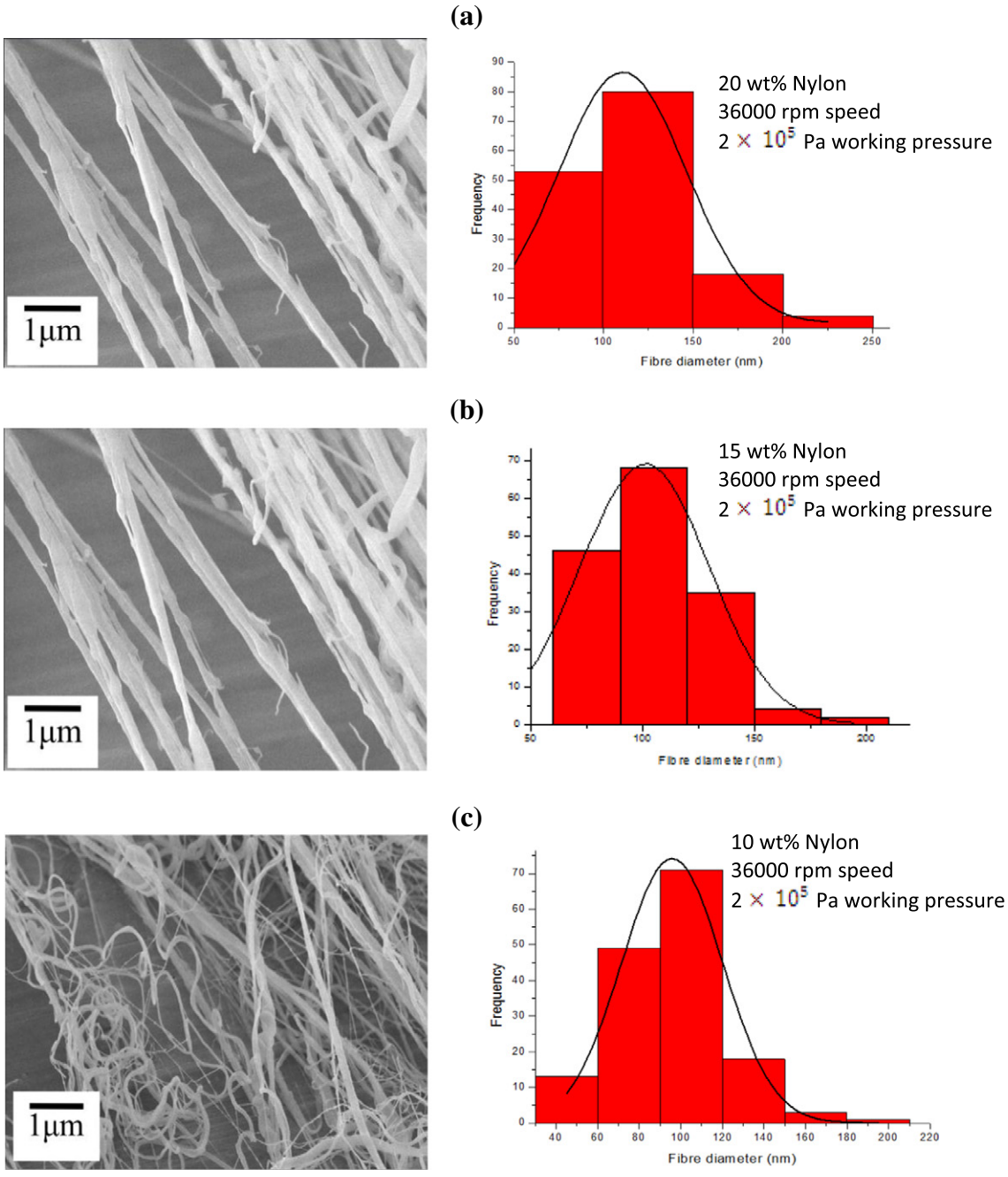

Fig. 2. (a)–(c) SEM images of nanofibres generated with 20 wt.%, 15 wt.% and 10 wt.% nylon solutions under different working pressures and maximum rotating speed (36,000 rpm) and corresponding fibre diameter distributions.

141 nm to 75 nm for 15 wt.% and 10 wt.% nylon solutions, respectively. The 5 wt.% nylon solution formed fibres at higher working pressures (0.2 MPa and 0.3 MPa) compared to lower working pressure. It is an interesting observation and associated with the pressure difference at the orifice which couples with centrifugal force to initiate fibre formation. Similarly, the Ag-loaded 5 wt.% nylon solutions also showed a reduction of fibre diameter with working pressure.

The change in fibre diameter is influenced by the combined effects of concentration of polymer, the rotating speed and the working pressure and these are summarised in Table 2. Firstly, there is a definite possibility of generating a larger fibre diameter at a higher polymer concentration, because a higher weight percentage of the polymer imparts higher viscosity and a lower solvent evaporation rate to the polymer solution. Secondly, the lack of centrifugal force and shear force at a low rotation speed can lead to a higher time constant of forces on the polymer solution, subsequently this results in a longer viscous response of the polymer solution to form thicker fibres. Thus, increasing the rotation speed will reduce the polymer fibre diameter. Meanwhile, at low polymer concentrations, in order to form fibres a minimum rotating speed is required to ensure the critical value of viscous response is reached [20]. Hence, there are only beads formed at a low rotating speed in the low concentration polymer solutions, but this situation can be changed by increasing the working pressure.

SEM images for the 20 wt.%, 15 wt.% and 10 wt.% of nylon fibres obtained under a fixed working pressure at 36,000 rpm speed and each corresponding fibre diameter distribution are shown in Fig. 2a–c. The fibres have straight, smooth and cylindrical morphology and they are bead-free in all instances. Previous electrospinning work has shown that higher viscosities favour bead free thicker fibres but increased surface tension encourages the formation of beaded fibres [26]. The increase of nylon concentration increased the viscosity of the polymer solution rapidly and was the main parameter controlling the

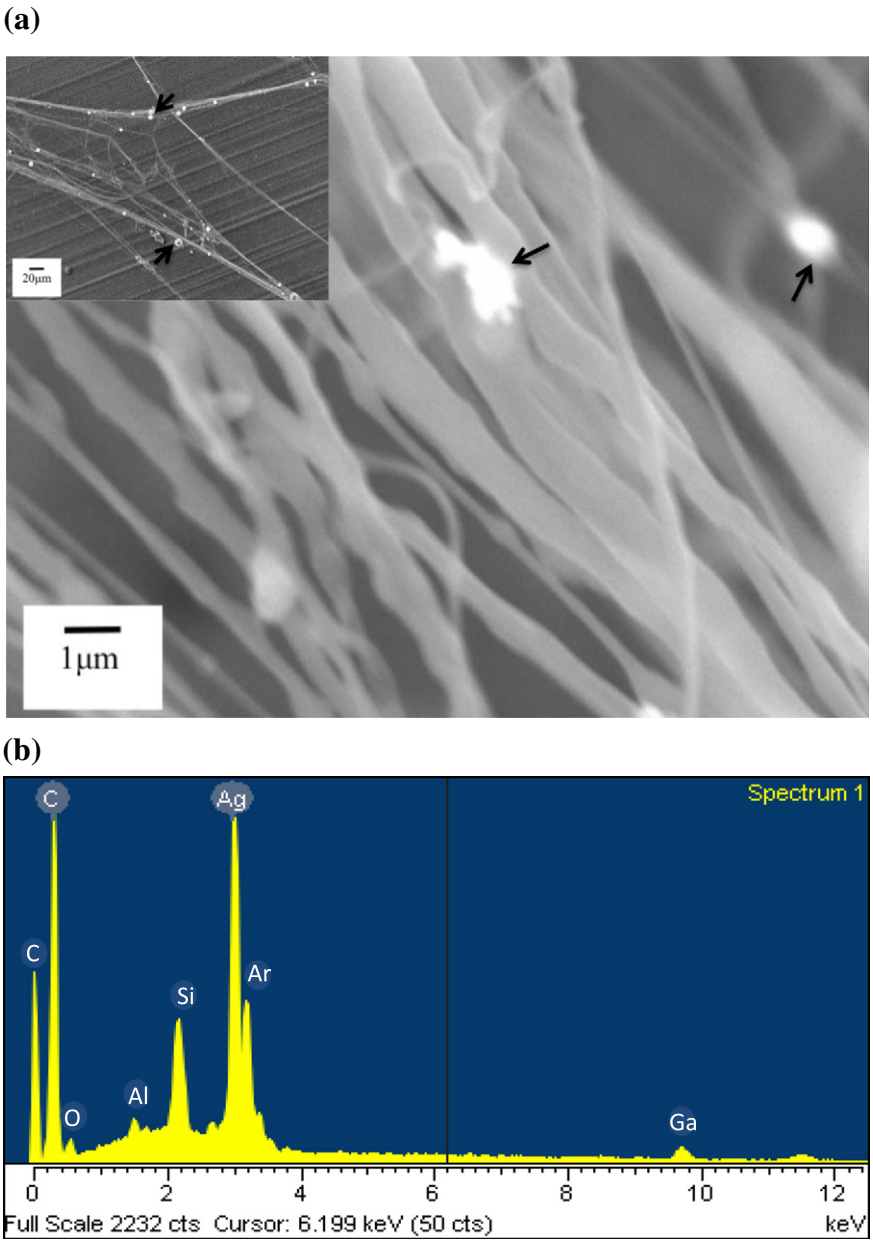

Fig. 3. (a) FE-SEM (FIB-SEM inset) micrograph showing that the Ag nanoparticles (see arrows) were present on nanofibres made using the 20 wt.% nylon–1 wt.% Ag suspension, and (b) the corresponding EDX analysis.

morphology of the formed fibres. It is also noteworthy that in dilute polymer solutions the polymer molecules have coil-like conformation and can be visualised as separated spheres. However, in the concentrated regime they form macromolecular entanglement which are crowded and touch with each other [27]. Thus, the increase of the viscosity promotes the occurrence of bead-free smooth fibre morphologies. Fig. 3a shows images of the Ag-loaded nylon nanofibres. Ag nanoparticles are clearly incorporated in nanofibres. EDX analysis was also performed to confirm the inclusion of Ag nanoparticles (Fig. 3b). Thus, pressurised gyration was successful in generating nanoparticle containing nanofibres.

Fig. 4a shows the Raman spectra of 20 wt.% nylon nanofibres. The Raman bands observed at 1600 cm^{-1}, 1436 cm^{-1} and 1371 cm^{-1} correspond to Amide I (C═O), CH_2 bending and CH_2 wagging, respectively. CH_2 twisting is shown at 1313 cm^{-1}. The peak at 1241 cm^{-1} is N–H wagging. The C–C–O stretch is identified at a peak 938 cm^{-1} [28]. Raman spectra for Ag-loaded nylon nanofibres are shown in Fig. 4(b) and (c). Fig. 4b represents the lower Ag concentration (i.e. 1 wt.%) and Fig. 4c denotes the higher Ag concentrations (i.e. 4 wt.%). The Raman band for C–H and N–H bonding is suppressed when the concentration of Ag increased in nylon nanofibres. However, the Amide I band (1600 cm^{-1}) is clearly seen in both spectra. In the case of Ag-loaded nanofibres Raman band of Amide I was shifted to higher wave number compared to the nylon nanofibres indicating that the Ag nanoparticles are bonded to nylon. The charge transfer between the nylon and the Ag nanoparticles are inevitable where nylon is partially positive and Ag is partially negative. This charge transfer effect indicates that the nylon and Ag are acting as donor and acceptor in the hybrid nanofibre system. Similar observations have been made for gold-loaded polyaniline nanofibres [29].

Fig. 5 summarises the deductions made from the ICP-MS study. Samples 1 and 2 show that there are no Ag ions to begin with in the stock solution, nitric acid, and in the de-ionised water, respectively. Samples 3, 4 and 5 represent the 1 wt.% Ag-loaded nylon nanofibres (20 wt.%) after undergoing 24, 48 and 72 h of washing, respectively. As expected, Ag ion concentration in the solution reduces after each washing cycle. The rate of Ag ion release after the first washing cycle is less compared to the second. This is also true for samples 6, 7 and 8 which are for 2 wt.% Ag-loaded nylon. Although samples 9, 10 and 11 (which are for 4 wt.% Ag-loaded nylon nanofibres) show a reduction in Ag ion concentration, the rate of ion release for consecutive washing cycles does not show a significant variation. These results show a similar trend to the results obtained with Ag ion release from polyamide 66 composites where faster release is observed in the initial period and subsequently the release abruptly slows down [30]. It is also clearly seen that the Ag ion concentration in the solution is higher after each cycle of wash for 4 wt.% Ag-loaded samples compared to the others. Sample 12 is for nylon nanofibres without any silver nanoparticles where no Ag ions are detected after a 72 h wash cycle. Effective antibacterial properties require a concentration level as low as 0.1 ppb and therefore the release of Ag ion from the hybrid system is sufficient even after a 72 h of washing [31].

The Ag ion release to an aqueous medium consists of three distinct steps. Initially, water molecules diffuse into the hybrid sample, then they will react with the Ag nanoparticles that eventually results in the formation and release of the Ag ions to an aqueous environment. The crystallinity and polarity of the matrix material influence the Ag ion release to an aqueous medium. These properties determine the level of diffusion barrier to water molecules and Ag ion release during mass transfer. The release characteristics of Ag ion in polypropylene were found to be influenced by crystallinity and water absorption potential of the polypropylene matrix [32]. Soaking time, concentration of silver powder, and silver specific surface area were identified as controlling factors in Ag ion release in polyamide [33]. A polyamide matrix has shown greater release potential than a polypropylene matrix due to

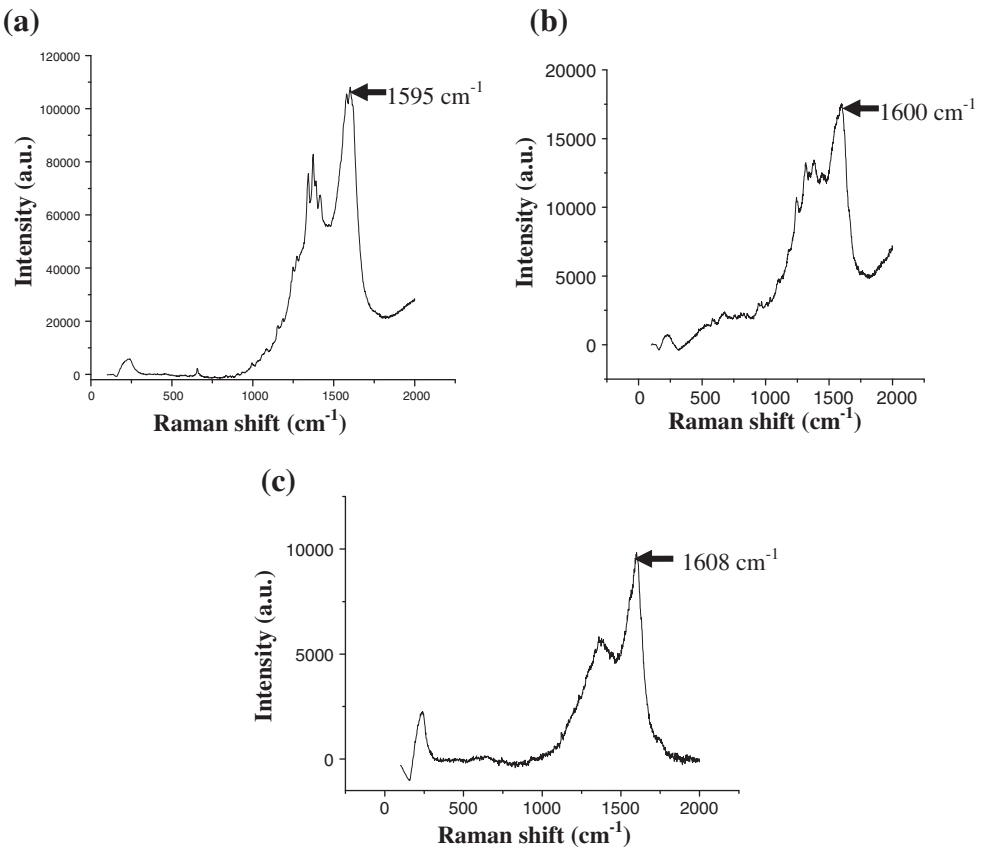

Fig. 4. Raman spectra (baseline corrected) for nanofibres (a) nylon (20 wt.%) (b) 1 wt.% of Ag–20 wt.% nylon (c) 4 wt.% of Ag–20 wt.% nylon. Arbitrary units are indicated by a.u.

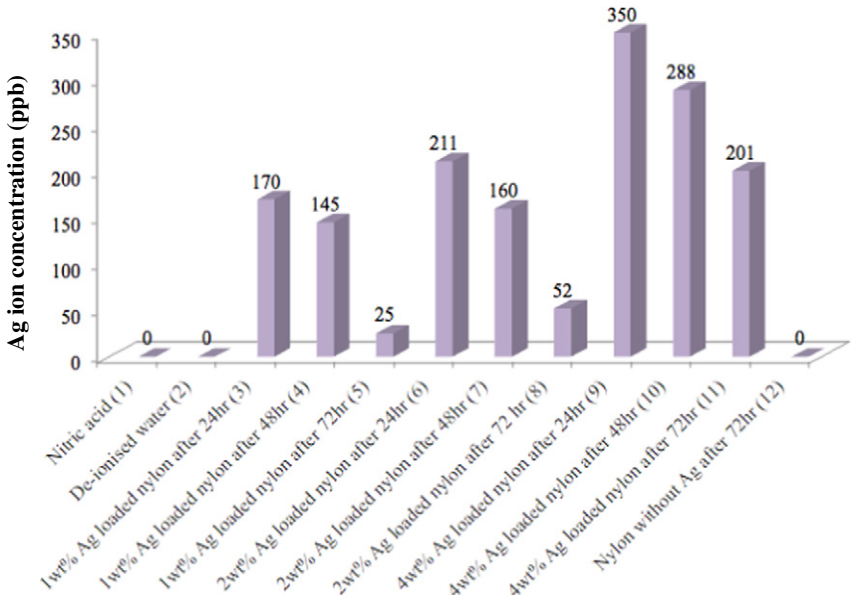

Fig. 5. Ag ion concentration in the nylon nanofibre mats (20 wt.% nylon) after 24, 48 and 72 h washing. Sample numbers are shown in brackets.

its inherent hygroscopicity [32,33]. The Ag ion release from the matrix is also influenced by the dissolution and swelling behaviour of the matrix polymer [34].

The rate of Ag ion release can include two mechanisms. Initially, Ag ions are released from the nanoparticles embedded in the surface of the nylon matrix. Secondly, when the washing or soaking time increases, the oxidation of interior Ag nanoparticles happens and subsequently Ag ion release can take place. The former is instantaneous and the latter occurs with prolonged time where water molecules have time to diffuse across many crystalline layers [35]. The onset of plasticisation and equilibrium sorption would impart a degree of mobility to the macromolecular chains and changes in the matrix region, and in this way Ag nanoparticles embedded within the matrix can get oxidised and release Ag ions over a prolonged time. In addition, polar groups in the nylon chains will be separated and induce water dipole interaction. This will provide a more flexible structure for Ag ion release [35]. It is also noteworthy that the thickness of the polymer matrix barrier decreases the Ag ion release and the barrier height and the hydrophobicity of the polymer matrix influence water uptake and the diffusivity of the molecules to the medium [36]. Moreover, mobility and the solubility of the water molecules in the polymer have to be taken into account during Ag ion release. Thus, for samples with a thicker barrier the water uptake is not sufficient to cause a high Ag ion release rate compared to samples with a thinner barrier height [37]. This shows that as the diameter of nanofibres changes in the chosen tested samples the Ag ion release rate also tends to change. This can promote an increase in the Ag ion release rate due to the barrier becoming thinner allowing easier penetration of (OH) molecules in exchange with Ag ions.

Antibacterial properties of the nanofibre samples were evaluated on Gram-negative *E. coli* and *P. aeruginosa* microorganisms. Five 20 wt.% nylon nanofibres, five 1 wt.% Ag-loaded 20 wt.% nylon nanofibres and two control groups were investigated with *E. coli* and *P. aeruginosa*, respectively. Fig. 6 shows the plots of antibacterial rate for *E. coli* and *P. aeruginosa* microorganisms after 2 h and 24 h. As the contact time increased the percentage of bacterial colonies reduced and plateaued for nylon nanofibres and Ag-loaded nylon nanofibres. The percentage reduction was higher for Ag-loaded nylon nanofibres than for the nylon nanofibres. There was no significant difference observed in percentage reduction after 2 h for Ag-loaded nylon nanofibres. However, nylon nanofibres showed reduced antibacterial activity after 2 h for both *E. coli* and *P. aeruginosa* microorganisms. Fig. 7 shows the bacterial cell proliferation and spreading after each of the time points for nylon

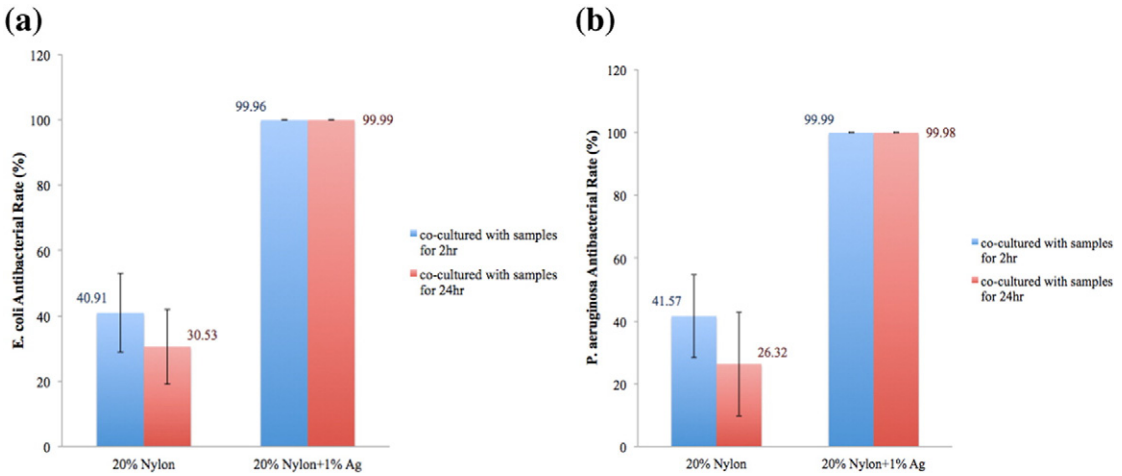

Fig. 6. Antibacterial rates of (a) *E. coli* at two time points; (b) *P. aeruginosa* at two time points.

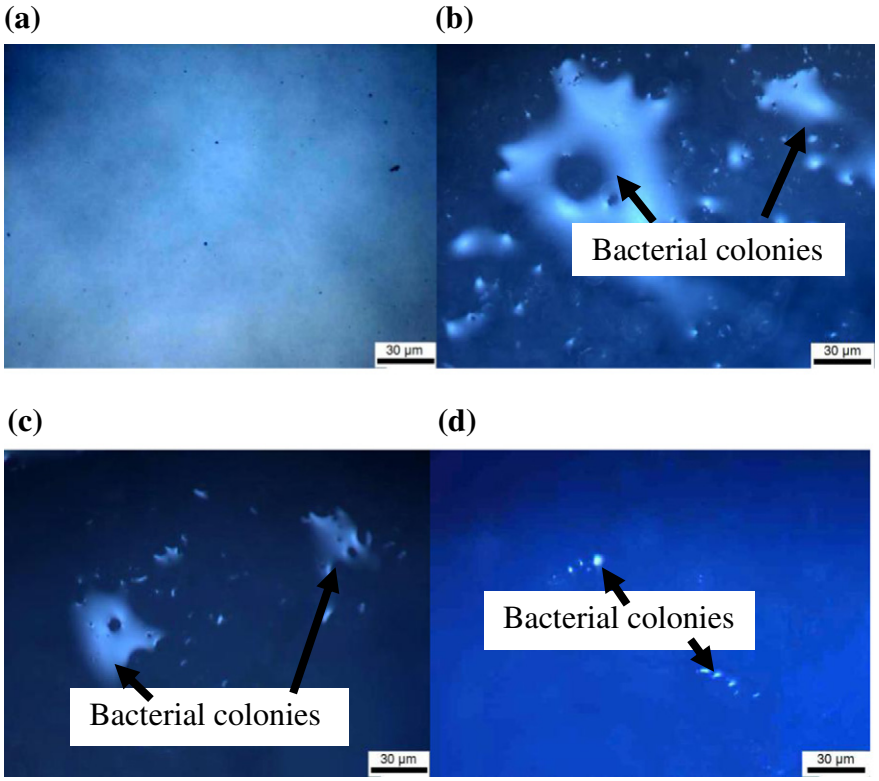

Fig. 7. Optical micrographs showing *E. coli* bacterial cells cultured in LB media (a) glass slide (control); (b) nylon nanofibres after 2 h; (c) nylon nanofibres after 24 h; (d) Ag-loaded nylon nanofibres after 2 h.

nanofibres and Ag-loaded nylon nanofibres. The nylon nanofibres contained a denser cell population than the glass slide and the Ag-loaded nylon nanofibres.

The mechanisms underlying the antibacterial activity of silver are not fully understood. Even though there are many reports proposing different mechanisms, there is no consensus. In the presence of Gram-negative bacteria, Ag nanoparticles attach to the cell walls and disturb cell wall permeability and cell respiration [34,38]. Other studies have shown that interaction between the Ag ions and the constituents of the bacterial membrane causes structural changes and damage in the cell membranes accompanied by intracellular metabolic activity, thus causing cell death [39]. The concentration of Ag nanoparticles and the formation of "pits" have also been proposed as the reason for the antibacterial activity, where the accumulation of Ag nanoparticles in the membrane caused permeability and the cell death [40,41]. Cell death was shown not to be caused directly by Ag nanoparticles but instead by Ag ion release from the Ag nanoparticles [42]. However, the fraction of metal that is bioavailable (that is, the actual amount which have entered into the cells) is the most important parameter, compared with percent dissolution of Ag nanoparticles that determines the efficiency of cell death [43]. The stronger electron storage capability of larger Ag nanoparticles is also found to impart excellent antibacterial activity [44]. The formation of free radicals influences cell lysis when the Ag nanoparticles are in contact with the bacteria. The free radicals have the ability to destroy the cell membrane and make porous surfaces which lead to cell death [45]. In addition, Ag ions released from the silver nanoparticles can react with the thiol groups of vital enzymes in the bacteria and inactivate them [46]. Such studies have also shown that the soft acidic form of Ag ions may react with soft bases in the cells such as sulfur and phosphorous which can cause cell death. DNA, for example, contains sulfur and phosphorous; when they react with Ag they become damaged ultimately leading to cell death [47]. Thus, although the exact mechanism responsible for antibacterial activity is to be resolved, and may be multifactorial, it is very clear that Ag-loaded nanofibres resulted in higher antibacterial activity than the virgin nylon nanofibres and the control groups, and that therefore, Ag contributed to cell death in *E. coli* and *P. aeruginosa*. As shown in the Ag ion release studies (ICP-MS), initially Ag nanoparticles in the matrix of the nylon have a significant effect on the antibacterial activity, and with increasing time, the nanoparticles embedded in the nylon will cause cell death.

4. Conclusions

Nylon and Ag-loaded nylon nanofibres were fabricated using a pressurised gyration process which has not been used before to fabricate antibacterial fibre mats. The process makes use of simultaneous centrifugal force and fluid flow blowing and evaporation to form the fibres. The fibre diameter generated was in the range of 50–500 nm. Key parameters such as vessel rotating speed, working pressure and polymer concentration had a significant effect on nanofibre diameter and morphology. The fibre diameter increased when increasing weight percentage of polymer, reduced with increasing vessel rotating speed and the process working pressure. Effective and proper incorporation of Ag nanoparticles into the nylon nanofibres was confirmed by advanced microscopy. The Raman spectra elucidated the bonding characteristics of nylon and the Ag nanoparticles. Ag ion release after repeated washing of the nanofibrous mats was detected by inductively coupled plasma mass spectroscopy which showed the Ag ion existence and concentration in the initial nanofibrous mats which influences the Ag ion release profile. A strong antibacterial-activity of Ag-loaded nylon was clearly demonstrated with bacterial killing rates reaching ~100% for Gram-negative *E. coli* and *P. aeruginosa* microorganisms.

Acknowledgements

The authors are grateful for an EPSRC-UCL Knowledge Exchange Programme Award which initiated this work and helped to attract privately

funded PhD researcher Zewen Xu. Dr. Mahalingam is supported by EPSRC grant EP/L023059/1.

References

[1] M. Lopez-Haro, T.G. Jiu, P. Bayle-Guillemaud, P.H. Jouneau, F. Chandezon, Multiscale tomographic analysis of polymer-nanoparticle hybrid materials for solar cells, Nanoscale 5 (2013) 10945–10955.

[2] L. Qiao, X. Wang, L. Qiao, X. Sun, X. Li, Y. Zheng, D. He, Single electrospun porous NiO–ZnO hybrid nanofibers as anode materials for advanced lithium-ion batteries, Nanoscale 5 (2013) 3037–3042.

[3] M. Montazer, S.B. Malekzadeh, Electrospun antibacterial nylon nanofibers through in situ synthesis of nanosilver: preparation and characteristics, J. Polym. Res. 19 (2012) 9980–9988.

[4] N. Vitchuli, Q. Shi, J. Nowak, K. Kay, J.M. Caldwell, F. Breidt, M. Bourham, M. McCord, Z.W. Zhang, Multifunctional ZnO/Nylon 6 nanofiber mats by an electrospinning–electrospraying hybrid process for use in protective applications, Sci. Technol. Adv. Mater. 12 (2011) 055004.

[5] M. Catauro, F. Bollino, F. Papale, S. Marciano, S. Pacifico, TiO_2/PCL hybrid materials synthesised via sol–gel technique for biomedical applications, Mater. Sci. Eng. C 47 (2015) 135–141.

[6] M. Yazdimamaghani, D. Vashaee, S. Assefa, K.J. Walker, S.V. Madihally, G.A. Kohler, L. Tayebi, Hybrid macroporous gelatin/bioactive-glass/nanosilver scaffolds with controlled degradation behaviour and antimicrobial activity for bone tissue engineering, J. Biomed. Nanotechnol. 10 (2014) 911–931.

[7] T. Amna, M. Shamshi Hassan, H. Van Ba, M.-S. Khil, H.-K. Lee, I.H. Hwang, Electrospun Fe_3O_4/TiO_2 hybrid nanofibers and their *in vitro* biocompatibility: prospective matrix for satellite cell adhesion and cultivation, Mater. Sci. Eng. C 33 (2013) 707–713.

[8] M. Ranjbar-Mohammaddi, S. Hajir Bahrami, M.T. Joghataei, Fabrication of novel nanofiber scaffolds from gum tragacanth/poly(vinyl alcohol) for wound dressing application: in vitro evaluation and antibacterial properties, Mater. Sci. Eng. C 33 (2013) 4935–4943.

[9] M.B. Bazbouz, G.K. Stylios, The tensile properties of electrospun nylon 6 single nanofibers, J. Polym. Sci. Polym. Phys. 48 (2010) 1719–1731.

[10] S. Sinha-Ray, Y. Zhang, A.L. Yarin, S.C. Davis, B. Pourdeyhimi, Solution blowing of soy protein fibers, Biomacromolecules 12 (2011) 2357–2363.

[11] J.H. Zhang, M.J. Markiewicz, B.P. Mowery, B. Weisblum, S.S. Stahl, S.H. Gellman, C-terminal functionalization of nylon-3 polymers: effects of C-terminal groups on antibacterial and hemolytic activities, Biomacromolecules 13 (2012) 323–331.

[12] L.F. de Oliveira, J.D. Goncalves, K.D. Goncalves, J. Kobarg, M.B. Cardoso, Sweeter but deadlier: decoupling size, charge and capping effects in carbohydrate coated bactericidal silver nanoparticles, J. Biomed. Nanotechnol. 9 (2013) 1817–1826.

[13] Z. Yang, Z.W. Liu, R.P. Allaker, P. Reip, J. Oxford, Z. Ahmad, G. Ren, A review of nanoparticle functionality and toxicity on the central nervous system, J. R. Soc. Interface 7 (2010) S411–S422.

[14] Z.W. Liu, T. Zhang, G. Ren, Z. Yang, Nano-Ag inhibiting action potential independent glutamatergic synaptic transmission but increasing excitability in rat CA1 pyramidal neurons, Nanotoxicology 6 (2012) 414–423.

[15] R.L. Williams, P.J. Doherty, D.G. Vince, G.J. Grashoff, D.F. Williams, The biocompatibility of silver, Crit. Rev. Biocompat. 5 (1989) 221–243.

[16] D. Guo, Y. Zhao, Y. Zhang, Q. Wang, Z. Huang, Q. Ding, Z. Guo, X. Zhou, L. Zhu, N. Gu, The cellular uptake and cytotoxic effect of silver nanoparticles on chronic myeloid leukemia cells, J. Biomed. Nanotechnol. 4 (2014) 669–678.

[17] H. Kong, J. Jang, Synthesis and antimicrobial properties of novel silver/polyrhodanine nanofibers, Biomacromolecules 9 (2008) 2677–2681.

[18] M. Guzman, J. Dille, S. Godet, Synthesis and antibacterial activity of silver nanoparticles against gram-positive and gram-negative bacteria, Nanomed-Nanotechnol, Biology, and Medicine 8 (2012) 37–45.

[19] M.S. Hassan, T. Amna, F.A. Sheikh, S.S. Al-Deyab, K.E. Choi, I.H. Hwang, M.-S. Khil, Bimetallic Zn/Ag doped polyurethane spider net composite nanofibers: a novel multipurpose electrospun mat, Ceram.Inter. 39 (2013) 2503–2510.

[20] S. Mahalingam, M. Edirisingh, Forming of polymer nanofibers by a pressurised gyration process, Macromol. Rapid. Comm. 34 (2013) 1134–1139.

[21] B.T. Raimi-Abraham, S. Mahalingam, M. Edirisinghe, D.Q.M. Craig, Generation of poly(N-vinylpyrrolidone) nanofibers using pressurised gyration, Mater. Sci. Eng. C 39 (2014) 168–176.

[22] S. Mahalingam, G.G. Ren, M. Edirisinghe, Rheology and pressurised gyration of starch and starch-loaded poly(ethylene oxide), Carbohyd. Polym. 114 (2014) 279–287.

[23] K.H. Liao, K.L. Ou, H.C. Cheng, C.T. Lin, P.W. Peng, Effect of silver on antibacterial properties of stainless steel, Appl. Surf. Sci. 256 (2010) 3642–3646.

[24] S. Mahalingam, B.T. Raimi-Abraham, D.Q.M. Craig, M. Edirisinghe, Langmuir 31 (2015) 659–666.

[25] S.L. Shenoy, W.D. Bates, H.L. Frisch, G.E. Wnek, Role of chain entanglement on fiber formation during electrospinning of polymer solutions: good solvent, non-specific polymer–polymer interaction limit, Polymer 46 (2005) 3372–3384.

[26] H. Fong, I. Chun, D.H. Reneker, Beaded nanofibers formed during electrospinning, Polymer 40 (1999) 4585–4592.

[27] C.B. Huang, et al., Electrospun polymer nanofibres with small diameters, Nanotechnology 17 (2006) 1558–1563.

[28] L.L. Cho, Identification of textile fiber by Raman microspectroscopy, Forensic. Sci. J. 6 (2007) 55–62.

[29] R.J. Tseng, et al., Charge transfer effect in the polyaniline-gold nanoparticle memory system, Appl. Phys. Lett. 90 (053101) (2007).

[30] X. Wu, J.D. Li, L. Wang, D. Huang, Y. Zuo, Y.B. Li, The release properties of silver ions from Ag-nHA/TiO_2/PA66 antimicrobial composite scaffold, Biomed. Mater. 5 (044105) (2010).

[31] Q. Shi, N. Vitchuli, J. Nowak, J. Noar, J.M. Caldwell, F. Breidt, M. Bourham, M. McCord, X. Zhang, One-step synthesis of silver nanoparticle-filled nylon 6 nanofibers and their antibacterial properties, J. Mater. Chem. 21 (2011) 10330–10335.

[32] C. Radheshkumar, H. Munstedt, Antimicrobial polymers from polypropylene/silver composites-Ag^+ release measured by anode stripping voltammetry, React. Funct. Polym. 66 (2006) 780–788.

[33] R. Kumar, H. Munstedt, Silver ion release from antimicrobial polyamide/silver composites, Biomaterials 26 (2005) 2081–2088.

[34] A.M. Abdelgawad, S.M. Hudson, O.J. Rojas, Antimicrobial wound dressing nanofiber mats from multicomponent (chitosan/silver-NPs/polyvinyl alcohol) systems, Carbohyd. Polym. 100 (2014) 166–178.

[35] R. Kumar, S. Howdle, H. Munstedt, Polyamide/silver antimicrobials: effect of filler types on the silver ion release, J. Biomed. Mater. Res-B 75B (2005) 311–319.

[36] N. Alissawi, V. Zaporojtchenko, T. Strunskus, T. Hrkac, I. Kocabas, B. Erkartal, V.S.K. Chakravadhanula, L. Kienle, G. Grundmeier, D. Garbe-Schonberg, F. Faupel, Tuning of the ion release properties of silver nanoparticles buried under a hydrophobic polymer barrier, J. Nanopart. Res. 14 (2012) 928–940.

[37] C. Damm, H. Munstedt, Kinetic aspects of the silver ion release from antimicrobial polyamide/silver nanocomposites, Appl. Phys A 91 (2008) 479–486.

[38] J. An, H. Zhang, J.T. Zhang, Y.H. Zhao, X.Y. Yuan, Preparation and antibacterial activity of electrospun chitosan/(polyethylene oxide) membranes containing silver nanoparticles, Colloid Polym. Sci. 287 (2009) 1425–1434.

[39] W.K. Jung, H.C. Koo, K.W. Kim, S. Shin, S.H. Kim, Y.H. Park, Antibacterial activity and mechanism of action of the silver ion in *Staphylococcus aureus* and *Escherichia coli*, Appl. Environ. Microbiol. 74 (2008) 2171–2178.

[40] I. Sondi, B. Salopek-Sondi, Silver nanoparticle as antibacterial agent: a case study on *E. coli* as a model for Gram-negative bacteria, J. Colloid. Inter. Sci. 275 (2004) 177–182.

[41] Y.Z. Zhou, J. Yang, T.T. He, H.F. Shi, X.N. Cheng, Y.X. Lu, Highly stable and dispersive silver nanoparticle–graphene composites by a simple and low-energy-consuming approach and their antimicrobial activity, Small 9 (2013) 3445–3454.

[42] Z.M. Xiu, Q.B. Zhang, H.L. Puppala, V.L. Colvin, P.J.J. Alvarez, Negligible particle-specific antibacterial activity of silver nanoparticles, Nano Lett. 12 (2012) 4271–4275.

[43] A. Ivask, A. Elbadawy, C. Kaweeteerawat, D. Boren, H. Fischer, Z. Ji, C.H. Chang, R. Liu, T. Tolaymat, D. Telesca, J.I. Zink, Y. Cohen, P.A. Holden, H.A. Godwin, Toxicity mechanisms in *Escherichia coli* vary for silver nanoparticles and differ from ionic silver, ACS Nano 8 (2014) 374–386.

[44] H.L. Cao, Y. Qiao, X. Liu, T. Lu, T. Cui, F. Meng, P.K. Chu, Electron storage mediated dark antibacterial action of bound silver nanoparticles: smaller is not always better, Acta Biomater. 9 (2013) 5100–5110.

[45] J.S. Kim, E. Kuk, K.N. Yu, J.-H. Kim, S.J. Park, H.J. Lee, S.H. Kim, Y.K. Park, Y.H. Park, C.-Y. Hwang, Y.K. Kim, Y.S. Lee, D.H. Jeong, M.-H. Cho, Antibacterial effects of silver nanoparticles, Nanomedicine 3 (2007) 95–101.

[46] Y. Matsumura, K. Yoshikata, S. Kunisaki, T. Tsuchido, Mode of bactericidal action of silver zeolite and its comparison with that of silver nitrate, Appl. Environ. Microbiol. 69 (2003) 4278–4281.

[47] J.R. Morones, J.L. Elechiquerra, A. Camacho, K. Holt, J.B. Kouri, J.T. Ramirez, M.J. Yacaman, The bactericidal effect of silver nanoparticles, Nanotechnology 16 (2005) 2346–2353.

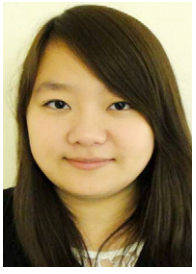

Zewen Xu gained a BEng in Mechanical Engineering from the University of Hertfordshire, UK and a Master of Engineering degree from the University of Newcastle, UK. Currently she is a PhD student in the Department of Mechanical Engineering at University College London. She is working in the Biomaterials Processing and Forming Laboratory where her research focuses on pressurised gyration of polymeric materials for antimicrobial applications.

Dr Suntharavathanan Mahalingam gained his doctorate from University College London (UCL). Subsequently, he was a research associate in the Interface Analysis Centre at Bristol University, UK. Currently, he is an Engineering & Physical Sciences Research Council (UK) supported research associate in the Department of Mechanical Engineering at UCL, where he is inventing techniques to manufacture functional polymeric fibres and smart bubbles across the scale range from micro-nano mainly for pharmaceutical and biomedical applications. He won the 2014 Materials Science & Engineering C Young Researcher Award.

Dr Jennifer Rohn is a Principal Research Associate at the Centre for Clinical Science and Technology in the Division of Medicine at University College London, UK. After earning a PhD in Microbiology from the University of Washington, Seattle USA, she did post-doctoral training at Cancer Research UK in London followed by a period in a start-up biotech company in the Netherlands, developing cancer therapeutics. Her current research focuses on understanding the biology and host/pathogen interaction of chronic urinary tract infection. She also investigates novel therapeutics and delivery systems.

Guogang Ren's research is focused on antiviral and antibacterial nanoparticles for biomedical and healthcare applications. He is also working on antimicrobial metals doped with functional nanoparticles that may contribute to new applications in biomedical devices, portable water purification and prevention of infectious disease spreading. His research also includes dispersing nanoparticles in bioengineering fluids, and their chemical conjugates.

Mohan Edirisinghe DSc holds the Bonfield Chair of Biomaterials in the Department of Mechanical Engineering at University College London. He has published over 300 journal papers and his most recent research is on creating novel techniques for the preparation of particles, bubbles, capsules and fibres. He has been awarded many prizes for his research including the Royal Society Brian Mercer Feasibility Award for an unprecedented three times (2005, 2009 and 2013).